JOURNAL OF MATERIALS SCIENCE 26 (1991) 4445–4454

Microstructure and origin of cross-tie fibrils in crazes

P. MILLER*, D. J. BUCKLEY, E. J. KRAMER
Department of Materials Science and Engineering, and the Materials Science Center, Cornell University, Ithaca, New York 14853, USA

Crazes were grown in thin films of polystyrene (PS) at various temperatures and the resulting craze fibril microstructures were examined using low-angle electron diffraction (LAED). A quasi-regular array of cross-tie fibrils pull the main fibrils away from the tensile axis by an angle $\pm \beta/2°$. As a result, the LAED patterns from crazes grown at temperatures $T < 50\,°C$ exhibited split diffraction lobes centred about the equatorial axis of the LAED pattern. It was found that β decreased with increasing crazing temperature and that the split lobes could no longer be resolved at the highest temperatures. Diffuse meridional diffraction spots due to scattering from the quasi-regular array of cross-tie fibrils were seen in the LAED patterns from crazes grown at low temperatures. The spacing of the cross-tie fibrils, R, determined from these patterns, was found to increase with the crazing temperature. A new model of craze widening was proposed that accounts for the formation of cross-tie fibrils by allowing some of the entangled polymer strands which bridge two fibrils in the active zone to survive fibrillation. Cross-tie fibrils are created when several such strands pile up locally, and the craze/bulk interface bypasses the pile-up.

1. Introduction

The fracture of glassy polymers in tension can be traced to the formation of crazes, highly localized regions of plastic deformation [1–4]. Crazes derive their name from their optical resemblance to microcracks. Examination in transmission electron microscopy (TEM), however, reveals a forest of highly drawn polymer fibrils which span the two craze/bulk interfaces. These fibrils allow the craze to support a load. Local fibril breakdown can create sites for crack nucleation which will grow slowly by the rupture of neighbouring fibrils. Eventually a crack of critical size will form and cause catastrophic failure of the sample.

A model for craze tip advance resulting from a meniscus instability mechanism has been proposed [5]. In this model, the strain-softened polymer just ahead of the craze tip is described as a non-Newtonian fluid. The applied stresses causes the fluid–air meniscus to advance. However, instabilities in the meniscus create finger-like voids. The fibrils are formed from the material between the voids as the meniscus advances.

Crazes grown in air widen by drawing fresh material into the fibrils from the active zone, a layer of strain-softened polymer approximately 25 nm wide at the craze/bulk interface [4, 6]. Entangled polymer strands in the active zone which bridge two fibrils typically either disentangle or break as the craze widens. At room temperature, chain scission is the dominant mechanism for the loss of entanglements with about one half of the entangled strands broken during fibrillation [4, 7]. Chain disentanglement becomes more important at temperatures close to the glass transition temperature, T_g [8].

The previous model is an extreme one in that it assumes that all the entangled strands which bridge two fibrils must break or disentangle. This mechanism would lead to a column-like fibril structure with no interconnections between the fibrils. High-resolution transmission electron microscopy shows that the true fibril microstructure is more mesh-like; there exists a large number of short cross-tie fibrils which bridge neighbouring main fibrils [9].

The existence of the extensive array of cross-tie fibrils in a craze is demonstrated dramatically in Fig. 1. Fig. 1a is a transmission electron micrograph of a crack which has propagated down the length of a craze. As is typical in this type of failure, the crack has propagated along one of the craze/bulk interfaces and then shifted to the other interface [10, 11]. The remnants of the fibrillated craze structure can be seen in Fig. 1a running diagonally from one side of the crack to the other. An enlargement of this feature is shown in Fig. 1b which clearly shows the fibrillated structure. This fibrillated region is laterally self-supporting; only the cross-tie fibrils are holding the remains of the craze together. Recently, Brown [12] has suggested that cross-tie fibrils are important in transferring load from the interface between the bulk polymer and craze behind the crack tip to the fibrils in the centre of the craze at the crack tip, thus providing a physically

* *Present address*: The 3M Company, 201-1W-28, 3M Center, St Paul, MN 55144, USA.

0022–2461/91 $03.00 + .12

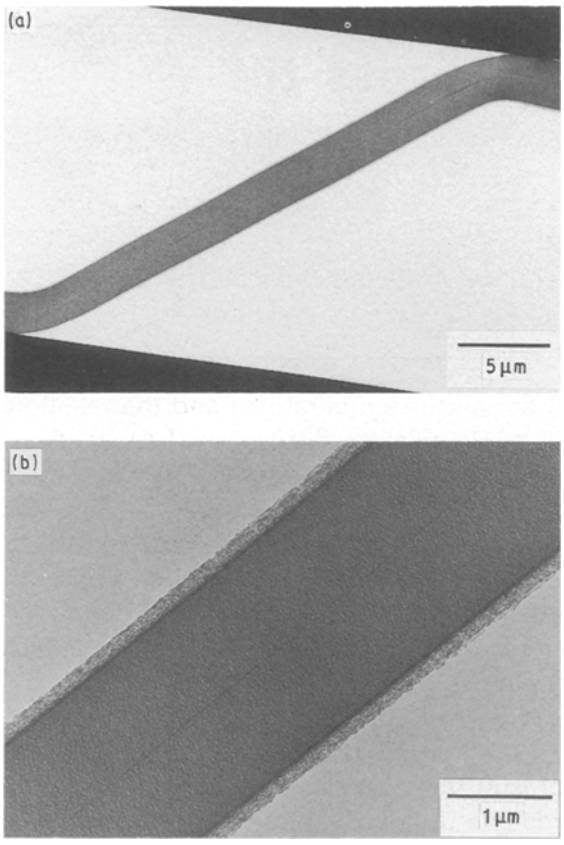

Figure 1 A transmission electron micrograph showing the remnants of the fibrillated material after a crack has propagated down a craze (a). A magnified view of the fibrillated material in (a) showing the fibril microstructure (b).

reasonable mechanism for a constant limiting crack opening displacement. Because the microstructure of the cross-tie fibrils will control this load transfer, information on this microstructure will be important for constructing realistic models for the micromechanics of fracture.

Previous work using low-angle electron diffraction (LAED) to characterize crazes has shown that the array of cross-tie fibrils in the craze gives rise to satellite diffraction spots implying that the arrangement of the cross-tie fibrils may be nearly periodic [13–15]. This paper reports an examination of the LAED patterns from polystyrene (PS) crazes as a function of temperature to quantitatively determine the underlying fibril microstructure. Particular attention was paid to the behaviour of the satellite diffraction spots and the angular distribution of the LAED intensity as a function of crazing temperature. From these results it was found that the cross-tie fibrils pull the main fibrils away from the tensile axis. A model to explain the origin of the cross-tie fibrils which can account for these results is proposed.

2. Experimental procedure

Nearly monodisperse PS with a molecular weight $M_w = 390\,000$, which had a polydispersity index $M_w/M_n < 1.2$, was used. Thin films (< 1.0 μm) of the PS were cast on glass slides by drawing at a constant rate from a methylene chloride solution. The films were cut into rectangular sections and floated off the slide on to the surface of a water bath. These sections were then picked up on annealed copper grids, the grid bars of which had been previously coated with PS. A brief exposure to methylene chloride vapour bonded the films to the copper grids.

The samples were placed in a vacuum oven (pressure $< 10^{-3}$ torr; 1 torr $= 1.333 \times 10^2$ Pa) and heated to 50 °C for 24 h to remove residual solvent and to age uniformly and physically the samples. Several suitable film squares were selected from each sample which contained few dust particles and no large defects. A small starter crack ~ 80 μm long was burnt into these film squares with a focused electron beam from a Joel 733 microprobe [16]. The grids were then mounted in a straining rig inside an oven and were strained at a constant strain rate of $4.2 \times 10^{-6}\ s^{-1}$. The temperature of the sample was monitored by a thermocouple in contact with the copper grid. The samples were strained to a total strain of approximately 0.06–0.09 at various temperatures to produce wide crazes suitable for LAED. At the completion of the run, the samples were quickly cooled by placing them in contact with a copper block at room temperature.

The samples were then examined by optical microscopy and a film square was selected that contained a single, isolated craze. This film square was carefully cut from the rest of the sample and mounted in a Joel 200 CX transmission electron microscope. The microscope was operated at an accelerating voltage of 200 kV using spot size 3. The LAED patterns were collected at a camera length of 51.8 m which had been previously calibrated from a carbon waffle grid of known spacing. An objective aperture 20 μm in diameter which served as a selected-area aperture was centred entirely within the craze when possible to avoid streaks in the LAED pattern which arise from refraction of the electron beam at the craze/bulk interface. Because it has been determined that the main fibrils coalesce as the craze ages [13], all of the samples were examined as soon as possible after they had been strained; in every case the delay was less than 30 min.

The LAED diffraction patterns thus obtained were scanned on a Joyce-Loebl microdensitometer 6 to determine the average fibril diameter and the cross-tie spacing. An RCI Trapix 5500 image processor was used to determine the angular breadth of the LAED patterns and to create false colour contour maps to show the splitting of the diffraction lobes and the satellite diffraction spots.

3. Results

Fig. 2a is a transmission electron micrograph of a craze grown at room temperature where the applied tensile stress lies along the y-axis in this orientation. Fig. 2b is an enlarged LAED pattern from this craze and is drawn schematically in Fig. 2c. The s_x- and s_y-axes in Fig. 2c correspond to the x- and y-axes, respectively, in Fig. 2a. The magnitude of the scattering vector, s, is given by

$$|s| = \frac{2\theta}{\lambda} \quad (1)$$

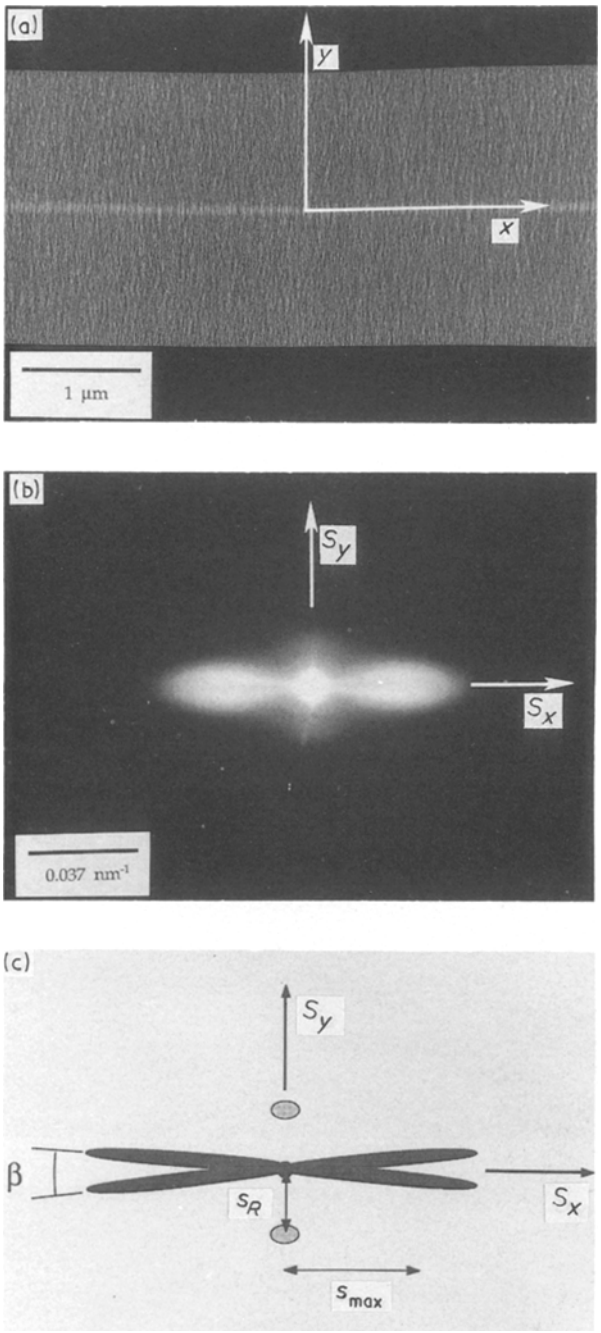

Figure 2 (a) A transmission electron micrograph of a typical craze grown in PS at room temperature. (b) An enlarged LAED pattern from a room-temperature craze. (c) A schematic drawing of an LAED pattern showing the angular separation between split lobes, β, and the position of the satellite diffraction spots.

where θ is the scattering angle and λ is the electron wavelength. The slit smeared intensity, $i(s_x)$, is determined by summing the intensity of the LAED pattern along lines parallel to s_y. The quantity s_{max} corresponds to the value of s_x for which $i(s_x)$ is a maximum.

Fig. 2b is a typical LAED pattern from a craze grown at low temperatures. This LAED pattern exhibits two diffraction streaks which lie on either side of the s_y-axis. Each streak is split into two lobes on either side of the s_x-axis. The splitting of the diffraction pattern produces a "dragon-fly wing" pattern which can be characterized by β, the angle of separation between the split lobes. The angle β is shown schematically in Fig. 2c. The existence of the split lobes indicates that the main fibrils do not lie parallel to the tensile axis; rather, the main fibrils occur along two preferred orientations which lie $\pm \beta/2$ from the tensile axis of the craze. In addition, secondary diffraction spots are seen lying at a distance s_R above and below the diffraction streaks on the s_y-axis. These diffraction spots, which are also shown in Fig. 2c, are typically diffuse and lie close to the central spot on the LAED pattern which make them very difficult to observe.

LAED patterns for PS strained at 23, 34, 51, 61 and 71 °C are shown in Fig. 3a–e, respectively. An image processor was used to create false colour intensity maps of these LAED patterns; black and white contour maps traced from these are shown in Fig. 4a–e. The satellite diffraction spots were enhanced in the contour images of the LAED patterns by subtracting a suitable fit to the background intensity of the transmitted electron beam.

The contour maps show that the split lobes become increasingly more difficult to resolve in the images of LAED patterns from crazes grown at higher temperatures; the LAED patterns and contour images from samples crazed above 50 °C do not show any indication of split lobes. Similarly, the satellite diffraction spots cannot be resolved in the LAED patterns or contour images of such patterns from crazes grown at high temperatures. Thus, the split lobes in the diffraction pattern from the main fibrils and the satellite diffraction spots from the cross-tie fibrils disappear as the crazing temperature is increased.

Another measure of the deviation of the main fibrils from the tensile axis can be made by determining the broadening of the LAED pattern intensity profile. Fig. 5a–e show the breadth of the LAED patterns from crazes grown at 23, 34, 51, 61, and 71 °C, respectively. These intensity profiles were taken along the line parallel to s_y at the value of $s_x = s_{max}$ and are plotted as a function of the angle from the s_x-axis of the LAED pattern. The full width at half maximum (FWHM) of the intensity profile is a measure of the breadth of the LAED pattern. These values are plotted in Fig. 6 as circles. This graph clearly shows the decrease in the breadth of the LAED pattern as the crazing temperature increases.

The two peaks from the split lobes evident in the LAED pattern from a craze grown at room temperature are also seen in Fig. 5a. The sum of two Gaussian curves was fit to the data and is shown as a dotted line in Fig. 5a. The angle between the split lobes, β, is determined as the angular distance between the centroids of the two Gaussian curves. When two distinct peaks could not be resolved in the intensity profile curves, the calculated curve was forced to fit at the intensity peak and to give the proper FWHM. This technique is advantageous because it allows β to be determined from LAED patterns which do not exhibit two well-defined intensity peaks. The calculated curves in Fig. 5 (dotted lines) reproduce the shape of the experimental intensity profiles (solid lines) reasonably well, providing some justification for this procedure. The triangles in Fig. 6 represent the values of β from the curves in Fig. 5a–e. The slopes from the

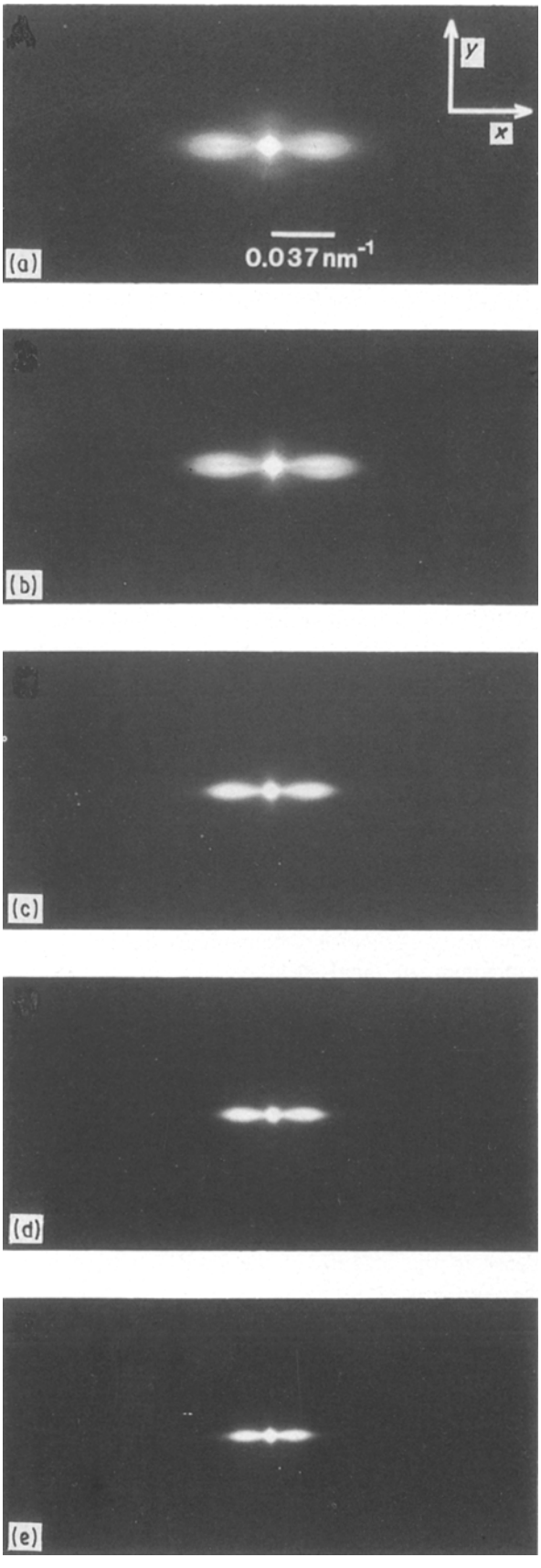

Figure 3 LAED patterns from crazes grown at (a) 23 °C, (b) 34 °C, (c) 51 °C, (d) 61 °C, and (e) 71 °C.

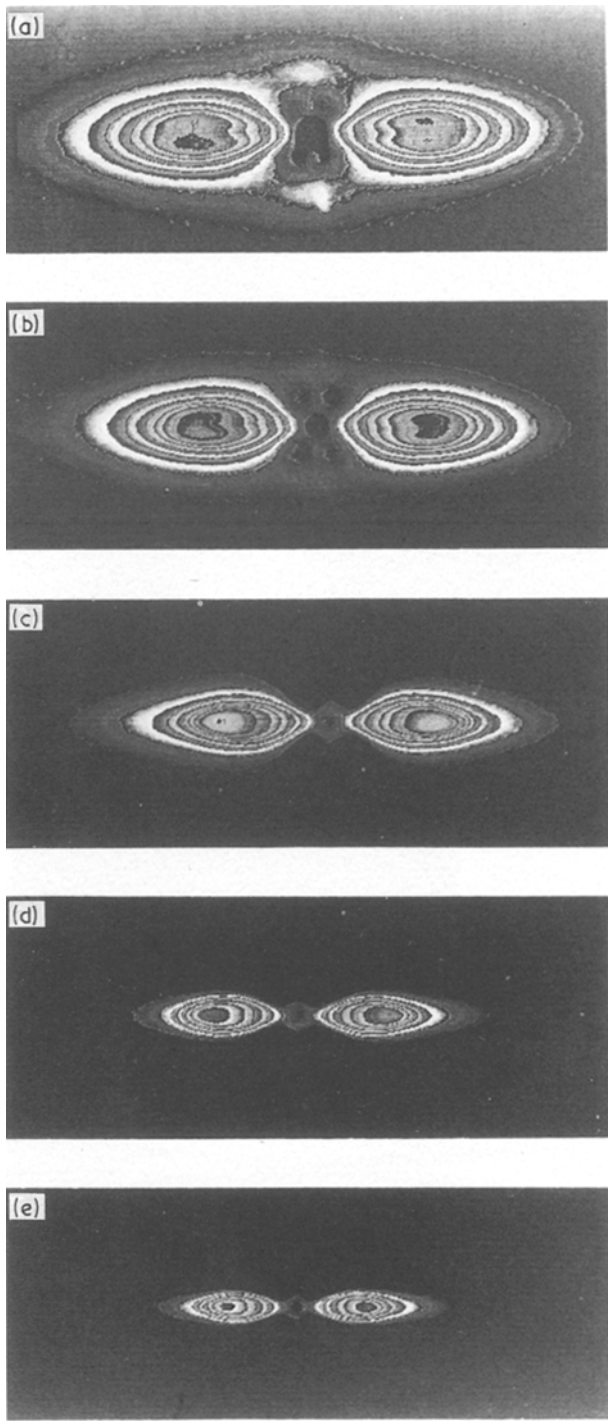

Figure 4 Contour maps of the LAED patterns in Fig. 3 from crazes grown at temperatures (a) 23 °C, (b) 34 °C, (c) 51 °C, (d) 61 °C, and (e) 71 °C. A Lorentzian background was subtracted from each image to enhance the satellite diffraction spots. The vertical streaks in contour maps (a) and (b) are due to refraction of the electron beam at the craze/bulk interfaces.

two data sets are identical within experimental error which indicates that the decrease in the breadth of the LAED pattern is due to the decrease in β even when two lobes cannot be directly resolved.

It is possible to directly determine the spacing, R, of cross-tie fibrils along the y-axis from the spacing of the satellite diffraction spots, s_R, using Bragg's law

$$R = \frac{1}{s_R} \tag{2}$$

The distance between the satellite spots is measured by scanning the microdensitometer along the y-axis of the LAED pattern. The background from the forward scattered beam is subtracted from the optical density

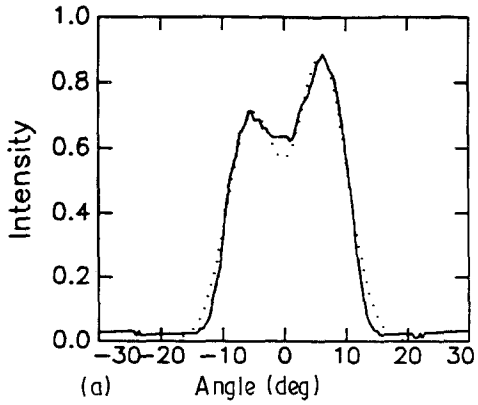

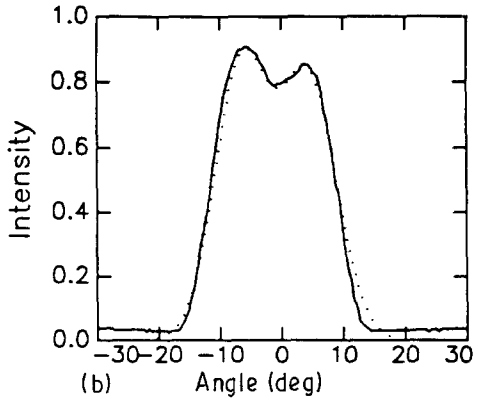

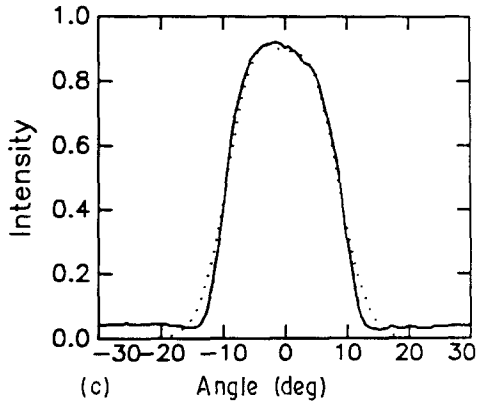

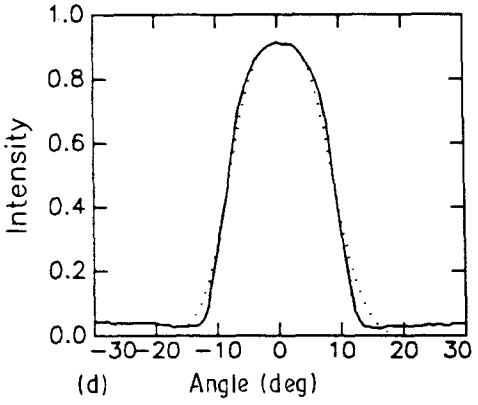

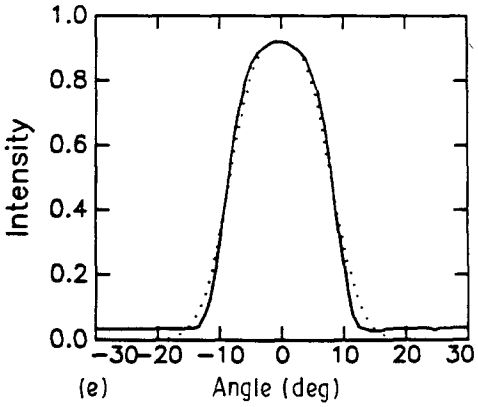

Figure 5 Intensity versus angular separation plots of the LAED patterns in the s_y direction at $s_x = s_{max}$ from crazes grown at temperatures (a) 23 °C, (b) 34 °C, (c) 51 °C, (d) 61 °C, and (e) 71 °C. (——). (– – –) The sum of two Gaussian curves which were fit to the data.

versus scattering vector curve and $2s_R$ is measured from background-corrected curve. Substituting these values into Equation 2 yields the spacing between the cross-tie fibrils. These data are plotted in Fig. 7 as a function of temperature. It is apparent from this plot that the cross-tie fibril spacing increases with increasing temperature.

It is possible to determine the average fibril diameter of a craze by performing a Porod analysis on the LAED pattern [17, 18]. The average fibril diameter, D, of the craze is determined from

$$D = \frac{\langle D^2 \rangle}{\langle D \rangle} = \frac{Q}{\pi^3(1 - v_f)k_1} \quad (3)$$

where k_1 is the Porod constant, Q is the scattering invariant, and v_f is the volume fraction of fibrils in the

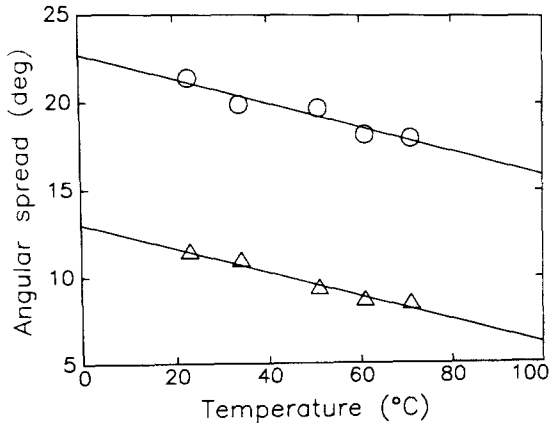

Figure 6 A plot of (○) the FWHM of the intensity profiles in Fig. 5 and (△) the angular separation of the split lobes, β, as a function of temperature.

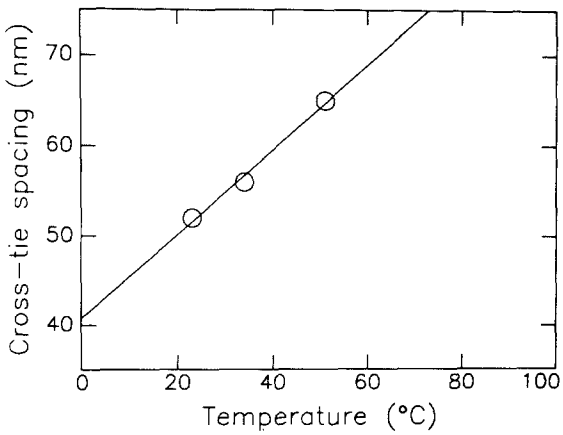

Figure 7 A plot of the spacing between cross-tie fibrils as a function of the crazing temperature.

craze which is known from previous work. It has been determined that inelastic electron scattering does not significantly alter the LAED pattern at large values of s and thus does not affect the values of D determined by Equation [14].

The Porod constant is given by

$$i(s_x) = k_1/s_x^3 \quad (4)$$

and the scattering invariant is determined from

$$Q = 2\pi \int_0^\infty s_x i(s_x) \mathrm{d}s_x \quad (5)$$

In practice, it is not possible to integrate the slit smeared intensity to infinity because $i(s_x)$ is only known to a maximum scattering vector, s_p. By re-writing Equation 5 as

$$Q = \int_0^{s_p} s_x i(s_x) \mathrm{d}s_x + \frac{2\pi k_1}{s_p} \quad (6)$$

it is possible to accurately determine Q from a LAED pattern of finite size. In order for Equation 6 to be strictly accurate though, s_p must lie in the Porod regime (i.e. for $s_x > s_p$, $i(s_x) = k_1/s_x^3$).

It is possible to determine the average fibril spacing, D_0, from

$$D_0 = \frac{D}{(v_f)^{1/2}} \quad (7)$$

on the assumption that the density of the polymer in the craze fibrils is the same as that in the bulk [4]. Fig. 8a and b are plots of the average fibril diameter and the average fibril spacing, respectively, as a function of the crazing temperature. Both D and D_0 are relatively insensitive to the crazing temperature for $T < 50\,^\circ\mathrm{C}$, but increase markedly with the crazing temperature above this value. These data are in good agreement with previous LAED and small-angle X-ray scattering (SAXS) results obtained by Berger *et al.* [15] on crazes grown at high temperatures.

The increase in D and D_0 as the crazing temperature is increased is predicted by a model in which the strain-softened material at the craze/bulk interface is treated as a non-Newtonian fluid [4]. By solving for the fastest widening craze, it is possible to show that

$$D_0 = \frac{8\Gamma}{\kappa S_c} \quad (8)$$

where S_c is the crazing stress, κ is a constant, and Γ is the energy to create new fibril surface

$$\Gamma = \gamma + c\nu^{1/2} \quad (9)$$

where γ is the van der Waals energy of intermolecular separation, c is a constant, and ν is the entanglement density of the polymer glass. Although Γ decreases slightly at elevated temperatures*, the decrease in S_c dominates the high-temperature behaviour of D_0 in Equation 8. Thus, the average fibril spacing (and hence the average fibril diameter) is expected to increase with increasing crazing temperature as observed.

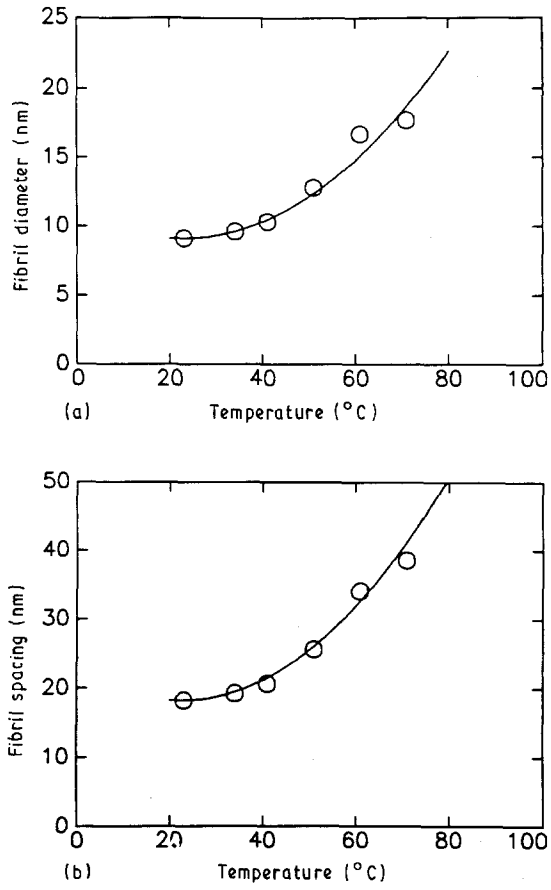

Figure 8 Plots of the average fibril diameter (a) and average fibril spacing (b) as a function of crazing temperature.

4. Discussion

4.1. Craze fibril microstructure

The fact that the LAED patterns from crazes grown at low temperatures exhibit split lobes indicates that there are two preferred orientations of the main fibrils which lie at angles $\pm\beta/2$ to the tensile axis†. This zig-zag structure is due to the cross-tie fibrils which pull the main fibrils away from the tensile axis. If the craze fibrils were infinitely long columns oriented exactly $\pm\beta/2$ from the tensile axis, the diffraction pattern would consist of two crossed lines centred about the s_x-axis separated by the angle β. Because the main fibrils have a finite length and because there is a distribution of orientations of the main fibrils centred about $\pm\beta/2$, the diffraction lobes have a finite breadth along the s_y-axis. Therefore, when β is small enough, the two lobes will overlap and will not be able to be resolved. This is the reason that the LAED patterns from the high-temperature crazes do not exhibit split lobes even though it has been determined that $\beta \neq 0°$ for these diffraction patterns.

Table I contains the measured values for D_0, D, β, and R at various crazing temperatures. The length of

* Enhanced disentanglement at high crazing temperatures reduces the number of chains which must be broken during fibrillation and thus decreases Γ.

† It is clear, however, that relaxation of the main craze fibrils in the direction perpendicular to the plane of the film is also necessary to account for the observed diffraction pattern, as first pointed out by Brown [12].

TABLE I The parameters describing the craze fibril microstructure at various crazing temperatures

Temp. (°C)	D_0 (nm)	D (nm)	β (deg)	R (nm)	l_f (nm)
23	18.2	9.1	11.4	52	7.4
34	19.2	9.6	10.9	56	7.8
41	20.6	10.3	10.2[a]	60[b]	8.5
51	25.6	12.8	9.3	65	11.2
61	34.1	16.7	8.6	69[b]	16.0
71	38.6	17.7	8.4	74[b]	19.4

[a] Determined from Fig. 6.
[b] Determined from Fig. 7.

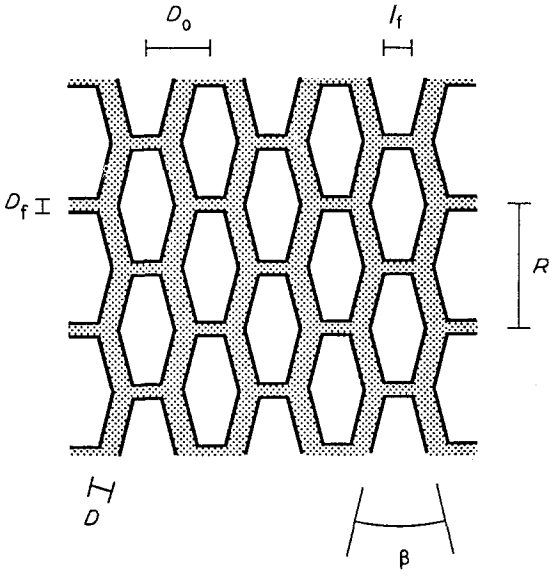

Figure 9 A schematic drawing showing the parameters which defined the craze fibril microstructure.

the cross-tie fibrils, l_f, can be determined once D_0, β, and R are known and the calculated values for l_f are also shown in Table I. Fig. 9 is a schematic illustration of the craze microstructure which defines these parameters. From geometrical considerations, an upper bound on the length of cross-tie fibril can be determined

$$(l_f)_{upper} = D_0 - D \quad (10)$$

We propose below that the cross-tie fibrils arise when the craze/bulk interface bypasses a pile-up of entangled strands which bridge two fibrils. Such a strand in the active zone would be nearly fully extended in the x-direction. Once the craze/bulk interface had bypassed the strand pile-up, the constraining stresses in the x-direction on the strands would be relieved and the chains in the cross-tie fibril would tend to relax from the extended configuration. Thus, it is expected that l_f will be somewhat shorter than the value predicted by Equation 10. Examination of the data in Table I shows that l_f is indeed slightly less than $(l_f)_{upper}$ over the entire range of temperatures examined. The contraction of the cross-tie fibrils pulls the main fibrils away from the tensile axis and accounts for the split diffraction lobes.

Using the data in Table I it is possible to construct the idealized fibril microstructure for crazes grown at various temperatures. Figs 10b and 11b represent the fibril microstructures for crazes grown at 23 and 51 °C, respectively‡. The angular separation of the main fibrils was allowed to deviate in these idealized drawings from the value of β listed in Table I by an amount ± FWHM/2 as determined from Fig. 6.

It is possible to test the accuracy of the idealized microstructures in Figs 10b and 11b by comparing them directly to crazes grown at the appropriate temperature. Figs 10a and 11a are high-resolution TEM micrographs of the fibril structure of crazes in thin films (~0.2 μm) of PS grown at 23 and 51 °C. TEM images are two-dimensional projections of three-dimensional structures, and the micrographs in Figs 10a and 11a represent several layers of fibrils overlaid on top of each other. Despite this complication, it is seen that the idealized microstructures in Figs 10a and 11b are reasonable approximations of the actual fibril microstructures displayed in the micrographs of Figs 10a and 11a, respectively, with the exception that the idealized microstructures are far more regular than the real structures.

4.2. The origin of the cross-tie fibrils

The model that describes craze widening assumes that any entangled strand which spans two fibrils must either disentangle or break during fibrillation [4]. While this model can only predict column-like fibrils with no interconnections, a simple modification of it can account for the rather regular formation of the cross-tie fibrils observed experimentally. Occasionally, an entangled polymer strand which bridges two fibrils in the active zone will not break or disentangle as the craze widens. As the craze continues to widen, such a strand will be pushed ahead of the craze/bulk interface in the active zone. If several such strands pile up locally, it will be energetically unfavourable to break all the strands. The craze/bulk interface will bypass the entanglement pile-up and leave behind a cross-tie fibril that contains the entangled strands and connects two neighbouring main fibrils. However once the cross-tie fibril has formed, the constraining stresses parallel to the interface will be relieved and the strands in the cross-tie fibril will tend to relax, making the cross-tie fibril spacing slightly shorter than the original spacing between the main fibrils. As a result the main fibrils are pulled out of alignment with the tensile axis, producing the split-lobes of the LAED diffraction pattern. A schematic drawing showing various stages in this process of cross-tie fibril formation is shown in Fig. 12.

This modified model of craze widening can account for the increase in cross-tie spacing as the crazing temperature is increased. It is known that chain disentanglement during fibrillation occurs more readily at higher temperatures [8]. At higher temperatures there would be fewer strands bridging two fibrils in the

‡ It was assumed that the diameter of the cross-tie fibrils is the same as the main fibrils.

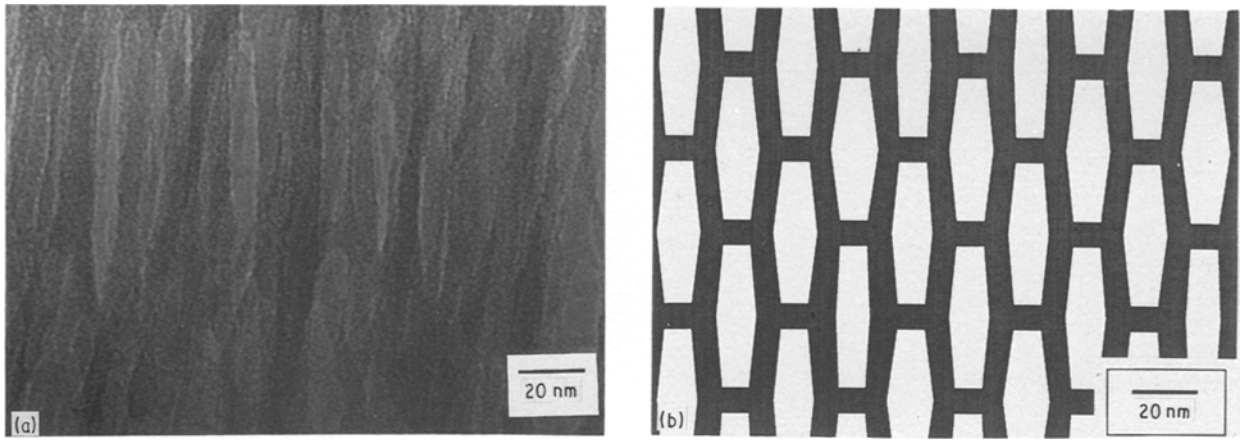

Figure 10 (a) A transmission electron micrograph of a craze grown at room temperature. (b) The idealized microstructure of a craze grown at room temperature.

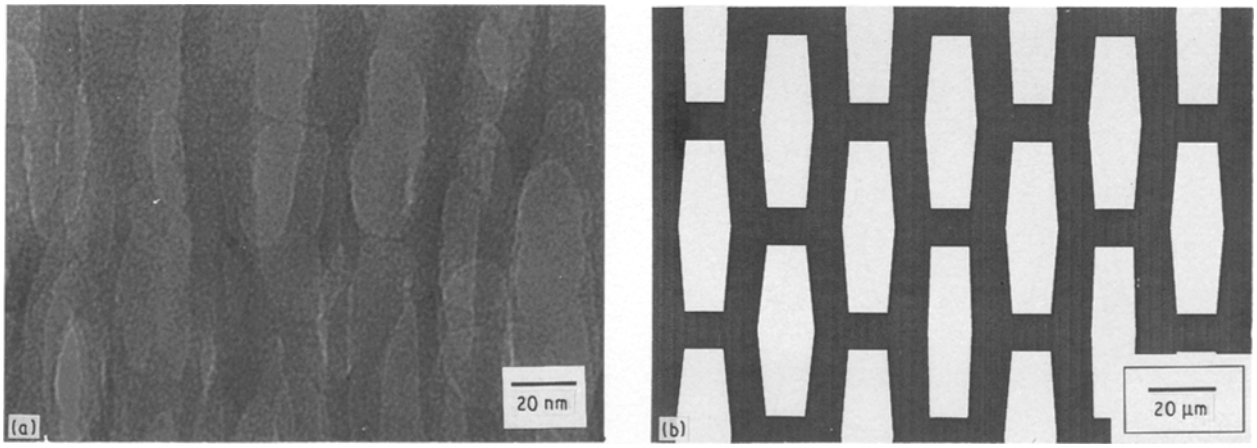

Figure 11 (a) A transmission electron micrograph of a craze grown at 51 °C. (b) The idealized microstructure of a craze grown at 51 °C.

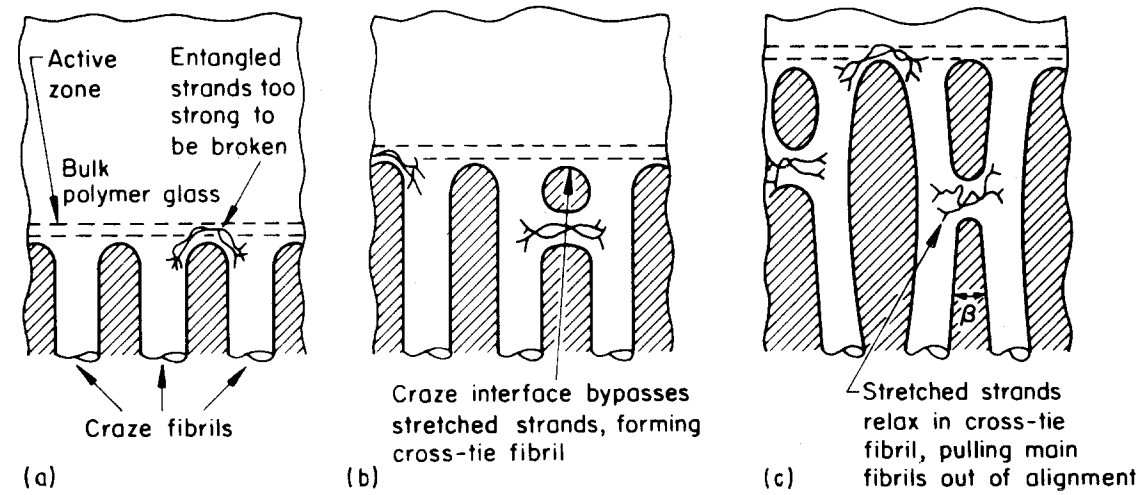

Figure 12 Schematic illustration showing the sequence leading to cross-tie fibril formation and relaxation.

active zone which would not disentangle during fibrillation and thus there would be fewer cross-tie fibrils formed. As a natural consequence, the spacing between cross-tie fibrils would increase with increasing crazing temperature. This increase in R, in turn, would cause a decrease in β.

Any other change in the polymer which produces a decrease in the density of entangled strands should also decrease β. Such changes have been observed. For example Yang *et al.* [19] found that diluting the strands in the entanglement network by adding polymer molecules too short to entangle led both to fewer cross-tie fibrils and to decreases in the angle β. Berger [20] showed that there was an excellent correlation between the entanglement density of a variety of polymers and polymer blends and the fibril misalignment; the smaller ν, the smaller was the angle β. Finally a recent study of the effect of preorientation of polymer

glass on craze microstructure found that if the pre-orientation direction was parallel to the craze fibrils, there were both fewer cross-tie fibrils and more nearly parallel alignment of the main fibrils than if the pre-orientation direction was perpendicular to the fibril direction [21]. This result is also what is expected from the model of cross-tie fibril formation presented above.

A common assumption in previous models of the fibril formation process is that all strands which cross the boundaries of a so-called phantom fibril (the bulk polymer that is drawn to become the fibril) must either disentangle or break. Clearly if some of these strands become incorporated into the cross-tie fibrils, this assumption is no longer strictly true and it is therefore important to examine how serious an error it produces. In the Appendix we estimate that p_{act}, the actual fraction of strands in the network that must be broken during fibrillation, is given by

$$p_{act} = [1 - (1 - p)(1 + p_c)] \quad (11)$$

where p is the fraction of strands which will break if there are no cross-tie fibrils and p_c is the ratio of the strands in the cross-tie fibrils to the strands in the main fibrils. We estimate p_c to be the ratio of cross-tie fibril volume to main fibril volume. In PS where $p \approx 0.5$ and $p_c \approx 0.142$ at room temperature, we find that $p_{act} \approx 0.43$ from Equation 11. This result is not very different from the previous value for p (≈ 0.5) which does not account for the strands in the cross-tie fibrils. While total volume of polymer in the cross-tie fibrils is only about 15% of the total in the craze, the correction for the polymer in the cross-tie fibrils will be more important for polymers with higher entanglement densities and smaller distances between cross-tie fibrils.

In summary, the modified model for craze widening presented here is able to predict the existence of the cross-tie fibrils. In addition, this model is consistent with the observed increase in the cross-tie spacing, R, and the decrease in the angular separation of the split LAED lobes, β, at higher crazing temperatures.

5. Conclusions

1. The craze microstructure is characterized by a quasi-regular array of cross-tie fibrils which bridge the main fibrils.

2. The cross-tie fibrils prevent the main fibrils from lying parallel to the tensile axis; the main fibrils exhibit two preferred orientations which lie at angles $\pm \beta/2$ from the tensile axis of the craze.

3. The formation of cross-tie fibrils is explained by a modified model of craze widening in which some of the entangled polymer strands which bridge two fibrils in the active zone are not broken or disentangled during fibrillation. A cross-tie fibril is created when several such strands pile-up locally, and the craze/bulk interface bypasses the pile-up.

4. The spacing between cross-tie fibrils increases with increasing temperature and accounts for the decrease in the angular separation between the split LAED pattern lobes.

Acknowledgements

The support of this work by the Cornell Materials Science Center which is funded by the National Science Foundation, DMR-MRL is gratefully acknowledged. Philip Miller was supported by a fellowship provided by the Mobil Chemical Company.

Appendix

It is possible to determine the number of strands which must be broken during fibrillation using a phantom fibril model. In this model, the main fibrils are drawn from a phantom fibril whose diameter is the same as the spacing between the main fibrils, D_0. All the polymer strands which cross the interface of the phantom fibril are assumed to break or disentangle during fibrillation; the fraction of such strands is p. For crazes grown in PS at room temperature $p \approx 0.5$ based on this model [4, 7].

The model for craze widening proposed above relaxes the restriction that all polymer strands bridging two fibrils (i.e. crossing the boundary of a phantom fibril) must break. The ratio of the strands in the cross-tie fibrils to the strands in the main fibrils, p_c, is given by

$$p_c = \frac{N_c}{N_m} = \frac{V_c}{V_m} = \frac{\pi(D_f/2)^2 l_f}{\pi(D/2)^2 R} \quad (A1)$$

where N is the number of strands in the fibril, V is the volume of the fibril and m and c stand for the main fibrils and cross-tie fibrils, respectively. Examination of the micrographs in Figs 10a and 11a reveals that the diameters of the cross-tie fibrils and the main fibrils are approximately equal, and thus one determines that at room temperature, $p_c = 0.142$ from Equation A1.

The density of the strands that survive fibrillation in the main fibrils as defined in the phantom fibril model, ν_{eff}, is given by

$$\nu_{eff} = \nu(1 - p) \quad (A2)$$

where ν is the entanglement density of the polymer glass before deformation. Assuming the density of surviving strands is the same in the main fibrils and the cross-tie fibrils, one can write an expression for the total number of strands which survive fibrillation, N_{total}

$$N_{total} = \nu_{eff} V_m + \nu_{eff} V_c \quad (A3)$$

Because the volume of the cross-tie fibrils was ignored in the determination of ν_{eff}, the total density of surviving strands in the main fibrils and cross-tie fibrils, ν_{total} is given determined by dividing Equation A3 only by V_m

$$\nu_{total} = \nu_{eff} \frac{V_m}{V_m} + \nu_{eff} \frac{V_c}{V_m} \quad (A4)$$

which can be rewritten as

$$\nu_{total} = \nu_{eff}(1 + p_c) \quad (A5)$$

The total density of surviving strands in the main fibrils and cross-tie fibrils can also be written as

$$\nu_{total} = \nu(1 - p_{act}) \quad \text{(A6)}$$

where p_{act} is the actual fraction of entangled strands which do not survive fibrillation in the main fibrils and does not include the strands in the cross-tie fibrils. Equating Equations A5 and A6 and using Equation A2, p_{act} is determined to be

$$p_{act} = [1 - (1 - p)(1 + p_c)] \quad \text{(A7)}$$

which is Equation 11 in the text.

References

1. S. RABINOWITZ and P. BEARDMORE, *CRC Rev. Macromol. Sci.* **1** (1972) 1.
2. R. P. KAMBOUR, *J. Polym. Sci. Macromol. Rev.* **7** (1973) 1.
3. A. N. GENT, "The Mechanics of Fracture", Applied Mechanics Division, Vol. 19, edited by F. Erdogon (ASME, New York, 1976) p. 55.
4. E. J. KRAMER, "Microscopic and Molecular Fundamentals of Crazing", in "Advances in Polymer Science 52/53" (Springer-Verlag, Berlin, 1983) Ch. 1, p. 7.
5. A. M. DONALD and E. J. KRAMER, *Phil. Mag.* **43A** (1981) 857.
6. P. MILLER, PhD thesis, Cornell University (1987) Ch. 2.
7. C. C. KUO, S. L. PHOENIX, and E. J. KRAMER, *J. Mater. Sci. Lett.* **4** (1985) 459.
8. L. L. BERGER and E. J. KRAMER, *Macromol.* **20** (1987) 1980.
9. P. BEHAN, M. BEVIS and D. HULL, *Proc. Roy. Soc. Lond.* **A343** (1975) 525.
10. J. MURRAY and D. HULL, *Polymer* **10** (1969) 451.
11. B. D. LAUTERWASSER and E. J. KRAMER, *Phil. Mag.* **39A** (1979) 469.
12. H. R. BROWN, to be published.
13. A. C.-M. YANG and E. J. KRAMER, *J. Polym. Sci. Polym. Phys. Edn* **23** (1985) 1353.
14. *Idem, J. Mater. Sci.* **21** (1986) 3601.
15. L. L. BERGER, E. J. KRAMER, R. A. BUBECK and D. J. BUCKLEY, *J. Polym. Sci. Polym. Phys. Edn* **25** (1987) 1679.
16. A. M. DONALD and E. J. KRAMER, *J. Mater. Sci.* **16** (1981) 2967.
17. E. PAREDES and E. W. FISCHER, *Makromol. Chem.* **180** (1979) 2707.
18. H. R. BROWN, *Mater. Sci. Rep.* **2** (1987) 315.
19. A. C.-M. YANG, E. J. KRAMER, C. C. KUO, and S. L. PHOENIX, *Macromol.* **19** (1986) 2020.
20. L. L. BERGER, *ibid.* **22** (1989) 3160.
21. C. MAESTRINI and E. J. KRAMER, *Polymer*, **32** (1991) 609.

Received 1 May
and accepted 16 May 1990